Journal of Hydrology 597 (2021) 126156

Contents lists available at ScienceDirect

Journal of Hydrology

journal homepage: www.elsevier.com/locate/jhydrol

Research papers

Sub-regional groundwater storage recovery in North China Plain after the South-to-North water diversion project

Chong Zhang [a,b,h], Qingyun Duan [c,d,*], Pat J.-F. Yeh [e], Yun Pan [f,g], Huili Gong [f,g], Hamid Moradkhani [h,i], Wei Gong [a,b], Xiaohui Lei [j], Weihong Liao [j], Lei Xu [k], Zhiyong Huang [l], Longqun Zheng [f,g], Xueru Guo [m]

[a] *Institute of Land Surface System and Sustainable Development, Beijing Normal University, Beijing, China*
[b] *State Key Laboratory of Earth Surface Processes and Resource Ecology, Beijing Normal University, Beijing, China*
[c] *State Key Laboratory of Hydrology-Water Resources and Hydraulic Engineering, Hohai University, Nanjing, China*
[d] *College of Hydrology and Water Resources, Hohai University, Nanjing, China*
[e] *Discipline of Civil Engineering, School of Engineering, Monash University (Malaysia Campus), Malaysia*
[f] *Beijing Laboratory of Water Resources Security, Capital Normal University, Beijing, China*
[g] *State Key Laboratory Base of Urban Environmental Processes and Digital Modelling, Capital Normal University, Beijing, China*
[h] *Center for Complex Hydrosystems Research, The University of Alabama, Tuscaloosa, AL, USA*
[i] *Center for Complex Hydrosystems Research, Department of Civil, Construction, and Environmental Engineering, The University of Alabama, Tuscaloosa, AL, USA*
[j] *Sate Key Laboratory of Stimulation and Regulation of Water Cycle in River Basin, China Institute of Water Resources and Hydropower Research, Beijing, China*
[k] *State Key Laboratory of Information Engineering in Surveying, Mapping, and Remote Sensing, Wuhan University, Wuhan, China*
[l] *Department of Earth Sciences, The University of Hong Kong, Hong Kong, China*
[m] *Department of Statistics, Beijing Normal University, Beijing, China*

ARTICLE INFO

This manuscript was handled by J. Simunek, Editor-in-Chief, with the assistance of Hoori Ajami, Associate Editor

Keywords:
Groundwater recovery
Groundwater depletion
GRACE
South-to-North water diversion
North China Plain

ABSTRACT

The South-to-North water diversion Middle Route Project (MRP) is expected to alleviate the long-term groundwater storage (GWS) depletion in North China Plain (NCP) after the beginning of its operation in December 2014. This study aims to investigate the effect of MRP on GWS by comparing GWS changes before (2003–2014) and after (2015–2018) the MRP operation. The analysis was conducted by using groundwater level data from 617 wells in NCP, and then evaluated against satellite-based water storage data from Gravity Recovery and Climate Experiment (GRACE) and its Follow-On missions. On average in NCP, a decreasing trend of -19.1 ± 5.1 mm/yr was seen in GWS based on well observations during 2003–2014, but a recovery trend of $+1.8 \pm 0.7$ mm/yr was found during 2015–2018. The GWS recovery was most prominent in subregions where groundwater over-utilization had occurred in NCP. GRACE exhibited the capacity to detect the regional GWS depletion during 2003–2014, but difficult to distinguish the sub-regional GWS recovery during 2015–2018. The potential causes for GWS recovery were found to be complicated, not only caused by the reduction of groundwater pumping as accelerated by MRP-diverted water, but also the increasing precipitation recharge of aquifers and the enhanced management of groundwater system. The findings highlight that GWS in NCP has started a gradual transition from unsustainable depletion to sub-regional recovery as benefit from the MRP water diversion.

1. Introduction

Water resources in China are unevenly distributed as evidenced by a sharp South-to-North down gradient in precipitation from ~2000 to ~200 mm/yr. About half of the population and two-thirds of farmlands are located in Northern China where the water resources are only one-fifths of the national totals (Liu et al., 2001; Liu and Xia, 2004). The North China Plain (NCP, Fig. 1a), which has an areal size of 140,000 km^2, 350 million population and 10% of China's grain yield, depends heavily on groundwater (GW) for human water supply (Liu et al., 2008; Zheng et al., 2010). NCP can be divided into two major subregions according to the quaternary hydrogeological features (Cao et al., 2013;

* Corresponding author at: State Key Laboratory of Hydrology-Water Resources and Hydraulic Engineering, College of Hydrology & Water Resources, Hohai University, Nanjing 210098, China.

E-mail address: qyduan@hhu.edu.cn (Q. Duan).

https://doi.org/10.1016/j.jhydrol.2021.126156
Received 8 July 2020; Received in revised form 11 February 2021; Accepted 27 February 2021
Available online 5 March 2021
0022-1694/

Foster et al., 2004; Zhang et al., 2009): the Piedmont Plain (PP, 54,000 km^2) west-bordering by the Taihang Mountain, and the East-central Plain (ECP, 86,000 km^2) east-reaching the Bohai Gulf (Fig. 1a). Water supply in PP is mainly from the shallow unconfined aquifers, while ECP's water supply is from the deep confined aquifers as its shallow GW is brackish (Kendy et al., 2004; Zheng et al., 2010).

GW pumping provides ~70% of irrigation and ~60% of total water supply in NCP (Liu and Xia, 2004). Unsustainable over-exploitation of GW since 1970 s has resulted in a significant GW decline at 0.5 ~ 2.0 m/yr (Gong et al., 2018; Wang et al., 2018). Recent estimates of GW storage (GWS) depletion from well observations or Gravity Recovery and Climate Experiment (GRACE) satellite measurements ranged between −32.0 ~ −17.0 mm/yr (i.e., −4.5 ~ −2.4 km^3/yr) (e.g., Feng et al., 2013, 2018; Huang et al., 2015; Pan et al., 2017; Rodell et al., 2018; Xu et al., 2019; Zheng et al., 2020). GWS depletion is particularly severe near Beijing and Tianjin (due to intensive domestic and industrial uses) and the agriculture-dominated areas near Shijiazhuang and Hengshui (Fig. 1a) (Deng et al., 2018; Zhou et al., 2020). Numerous cones of depression (see Fig. S1 in the supplementary material) can be found near these cities with a maximum depth of >62 m in the unconfined aquifers and >110 m in the confined ones (Shang et al., 2016; Wang et al., 2018; Zheng et al., 2010).

To optimize water resources allocation and mitigate the "groundwater crisis" (Famiglietti, 2014), Chinese government constructed the world's largest water diversion project, the South-to-North water diversion project, to transfer water from the southern China via the Western, Middle and Eastern Routes (Liu and Zheng, 2002). The Middle Route Project (MRP, Fig. 1a) was designed to transfer 9.5 km^3/yr of water from the Danjiangkou Reservoir in the Hanjiang River basin to NCP. Since its operation in December 2014, MRP has delivered a total of 23.9 km^3 (2.3, 3.6, 4.8, 6.3 and 6.9 km^3/yr in 2015 to 2019 respectively) to NCP. About 24.8% and 20.0% of the diverted MRP water were

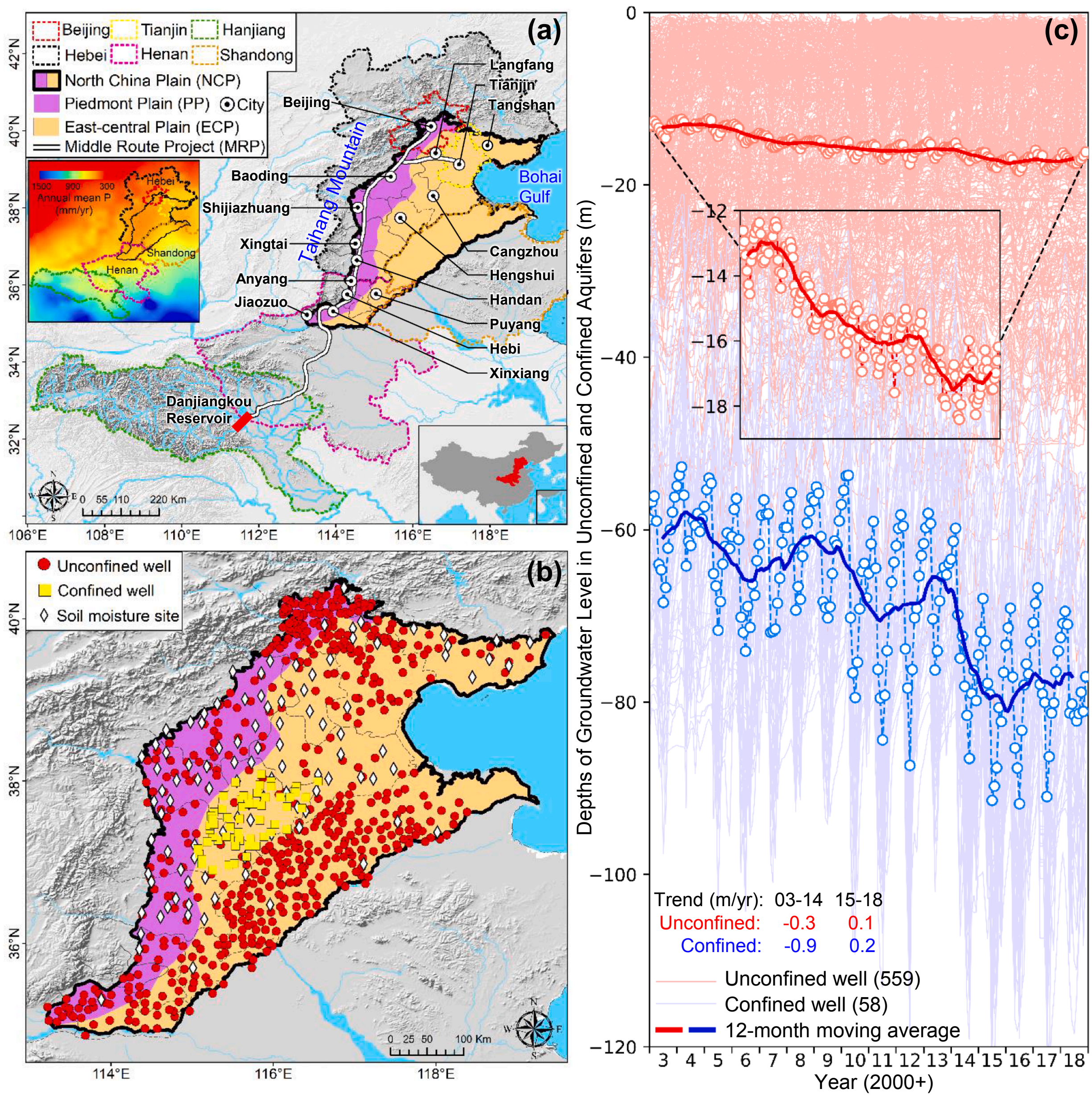

Fig. 1. (a) Overview of MRP for delivering water from the Hanjiang River basin to NCP. The inlet shows spatial mean precipitation distribution. (b) The observed networks of soil moisture (115 stations) and groundwater levels (in the 559 unconfined and 58 confined wells) are shown in different types and colours of markers. (c) The 2003–2018 mean groundwater level depths in the unconfined and confined aquifers are plotted with the 12-month moving average given. Also inserted is the unconfined groundwater levels zoomed in for better visualization. The clouds of thin lines are the groundwater level observed at each of the 617 wells.

allocated to Beijing and Tianjin, and the rest to other twelve cities (Fig. 1a and see Table S1 in the supplementary material). The water has been used for compensating environmental flow, replenishing reservoirs, recharging aquifers, and replacing urban GW pumping (He et al., 2019; Lei et al., 2018; Rogers et al., 2020). About 12,000 private wells were shut down along the MRP conveyance line, particularly at Hengshui, Cangzhou, Xingtai and Handan with a shutdown rate close to 100% (Gao et al., 2018). GW pumping has reduced considerably in those cities and for the entire NCP by ~1.3 km^3/yr during 2015–2017 (Fig. 1a and see Table S2).

Even with the successful commencement of MRP, one issue still under debate is whether MRP operation has already contributed to the recovery of GWS in NCP (Lei et al., 2018; Rogers et al., 2020; Yao et al., 2019). Most of the previous studies used regional GW modelling to demonstrate that MRP operation can increase soil moisture, evapotranspiration, and GW recharge (e.g., Shao et al., 2013, 2019; Shu et al., 2012; Ye et al., 2014; Zhang et al., 2018, 2020a; Zou et al., 2016). Beijing and Tianjin were identified with GWS recovery from modelling (Rogers et al., 2020; Wang et al., 2018; Zou et al., 2016), but in other parts of NCP the recovery remains elusive. For instance, GWS recovery in Shijiazhuang was modelled by Shao et al. (2013) and Zou et al. (2016), while Shu et al. (2012) and Ye et al. (2014) concluded that MRP can only alleviate GWS depletion without meaningful recovery. Although these previous modelling studies provided some divergent insights about the effect of MRP on GWS, most of them were not constrained by well observation and hence with considerable amounts of uncertainty (Long et al., 2020; Zhang et al., 2020b).

This study represents a first attempt to use the observed records of monthly GW levels from 617 wells during 2003–2018 to analyse the spatiotemporal GWS depletion and recovery in NCP. Two study periods, before (2003–2014) and after (2015–2018) the MRP operation, are identified (hereafter referred to as P1 and P2, respectively) for separate analyses. Potential causes for the changes of GWS trend in sub-regional distribution and magnitude are explored by using precipitation, MRP water diversion, GW pumping data. GWS estimates from well observation were compared to the corresponding monthly estimates from GRACE and GRACE Follow-On (GRACE-FO) data over NCP and four defined sub-regions. In contrast to previous studies that using GRACE data to investigate the GWS depletion in NCP, our work is based on the large amounts of long-term observed GW level data covering most of the entire NCP, and the focus here is on detecting the sub-regional GWS recovery and potential causes after the MRP operation.

2. Data and methodology

2.1. GWS estimation from well observation

The monthly GW level measurements from 617 wells (559 unconfined and 58 confined) during 2003–2018 were obtained from the Chinese GW management authority and the GW yearbook (ICGEM, 2018). The spatial distribution of the unconfined wells in NCP is more uniform than the confined wells that are available only near Hengshui and Xingtai (see the NCP data networks in Fig. 1b). Fig. 1c plots the 2003–2018 monthly time series of GW levels in 617 wells. Each well follows a strict quality control that it has >70% of coverage during the study period. Given the spatial non-uniformity in well distribution, the Thiessen polygon approach was used to determine the area weight of each well in estimating the regional mean GW level. It was observed that the mean GW levels in the unconfined and confined wells have declined by −0.3 and −0.9 m/yr during P1, and followed by a mild recovery of +0.1 and +0.2 m/yr during P2, respectively (Fig. 1c). GWS change was calculated by multiplying the area-weighted GW level changes by the specific yield for the unconfined wells or the storage coefficient for the confined wells (Zhang et al., 2009). The ranges of specific yield and storage coefficient in NCP are 0.025 ~ 0.290 and 0.0004 ~ 0.0045, respectively, which were also used in Cao et al. (2013) and Huang et al. (2015). More details on the Thiessen polygons for wells and the spatial distributions of specific yield and storage coefficient in NCP are given respectively in Figs. S2 and S3 in the supplementary material.

2.2. GWS estimation from GRACE data

The version 2 of GRACE (Jan 2003–Jun 2017) and GRACE-FO (Jun 2018–Dec 2018) RL06 mascon solution, processed by the Jet Propulsion Laboratory (JPL), was used to estimate monthly total water storage (TWS) changes (Landerer et al., 2020; Wiese et al., 2018). The JPL mascon solution used the regional concentration function to constrain mass variation, which is expressed in terms of the globally equal-area 3° × 3° spherical caps (Watkins et al., 2015). Though this solution provides TWS data in a spatial sampling of 0.5° × 0.5° resolution, the value of each grid cell in the same cap is identical. To reduce the leakage errors introduced by the mascon basis function, a set of scale factors with the 0.5° × 0.5° resolution derived from the Community Land Model (CLM) version 4.0 were used to calibrate GRACE TWS estimate (Wiese et al., 2016). More information on the data processing and leakage error reduction of the JPL mascon solution can be found in Watkins et al. (2015) and Wiese et al. (2016), respectively.

GRACE data contained a total of 18 months of data gaps during 2003–2017 and another 11-month gap (July 2017–May 2018) between GRACE and GRACE-FO. To fill these gaps, the approach of a seasonal-trend decomposition procedure based on Loess (STL, Cleveland et al., 1990) was applied to decompose the TWS time series into three components representing seasonal, trend and residual signals, respectively. The piecewise cubic Hermite interpolating polynomial (Fritsch and Carlson, 1980), which has the advantage of eliminating over- and undershot in interpolation, was used to fill the data gaps in the time series of three components. Three time series were then added back to reconstruct the TWS time series without data gaps. Applying these procedures to each grid cells provides the spatio-temporally continuous records of GRACE TWS data for the analysis in this study. A schematic on the processing of GRACE TWS data in one grid cell is given in Fig. S4.

The monthly in-situ soil moisture storage (SMS) data with the monitoring depth of 0.75 m were collected from 104 sites maintained by the China Meteorological Administration (Fig. 1b). Similar to the processing of GW level data, the Thiessen polygon approach was used to determine the area weight of each site for estimating the regional mean SMS change. Fig. S5 shows the spatial distribution of Thiessen polygons based on 104 SMS sites. Since the observed SMS data are only available during 2003–2013 and with some data gaps in winter seasons due to frozen soils, the SMS data taken from four Global Land Data Assimilation System (GLDAS) models (i.e., Community Land Model (CLM), Variable Infiltration Capacity (VIC), Noah and Mosaic) (Rodell et al., 2004) were used as an alternative to estimate SMS change. The soil depths in the four GLDAS models are 3.433 m (CLM), 3.5 m (Mosaic), 2.0 (Noah), and 1.9 m (VIC), respectively. Four GLDAS models perform simulation at the spatial resolution of 1° × 1° (Rodell et al., 2004). To be consistent with the resolution of GRACE TWS, the simulated data of four GLDAS models are resampled to 0.5° × 0.5°.

Fig. 2 plots the comparison of monthly time series of regional mean SMS between in-situ observation and four GLDAS model simulations in NCP during 2003–2013. For the consistency with the observed soil depth, only the GLDAS SMS data for the upper 0.75 m were used. As shown in Fig. 2, the CLM SMS is selected for subsequent analysis because it has the highest correlation coefficient (R = 0.67) and smallest root-mean-square error (RMSE = 9.3 mm) with the observed SMS among GLDAS models. Due to the lack of the observational data of snow water equivalent (SWE) and canopy water storage (CWS) changes in NCP, the data of SWE and CWS simulated by CLM were used in subsequent analysis.

TWS is the summation of individual components, including SWE, CWS, SMS, GWS and surface water storage (Rodell et al., 2018). Changes of surface water storage in lakes, wetlands, reservoirs, and rivers are

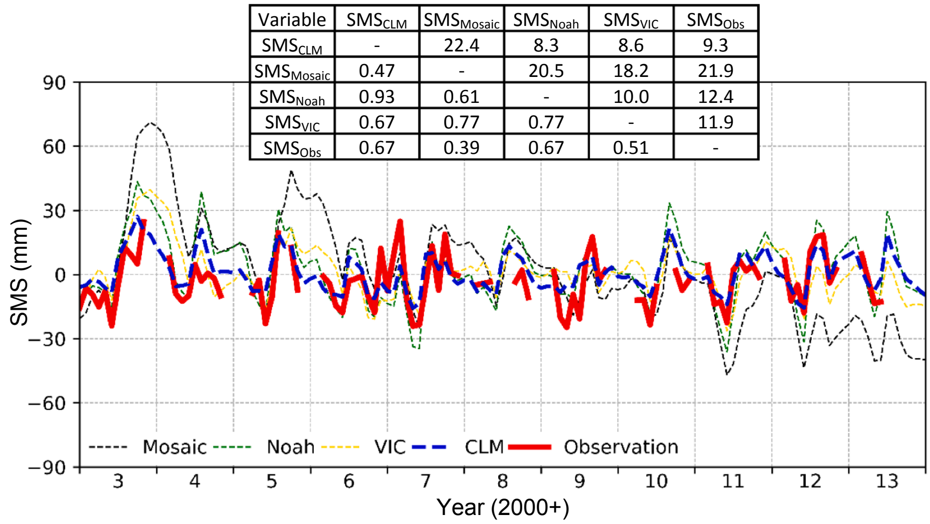

Variable	SMS_{CLM}	SMS_{Mosaic}	SMS_{Noah}	SMS_{VIC}	SMS_{Obs}
SMS_{CLM}	-	22.4	8.3	8.6	9.3
SMS_{Mosaic}	0.47	-	20.5	18.2	21.9
SMS_{Noah}	0.93	0.61	-	10.0	12.4
SMS_{VIC}	0.67	0.77	0.77	-	11.9
SMS_{Obs}	0.67	0.39	0.67	0.51	-

Fig. 2. Comparison of 2003–2013 monthly SMS simulated by four GLDAS models (CLM, VIC, Mosaic, and Noah) with the in-situ observations in NCP. The correlation coefficient (R) and root-mean-square error (RMSE, mm) of comparisons are also given in the lower-left and upper-right part of the inserted matrix in this figure, respectively.

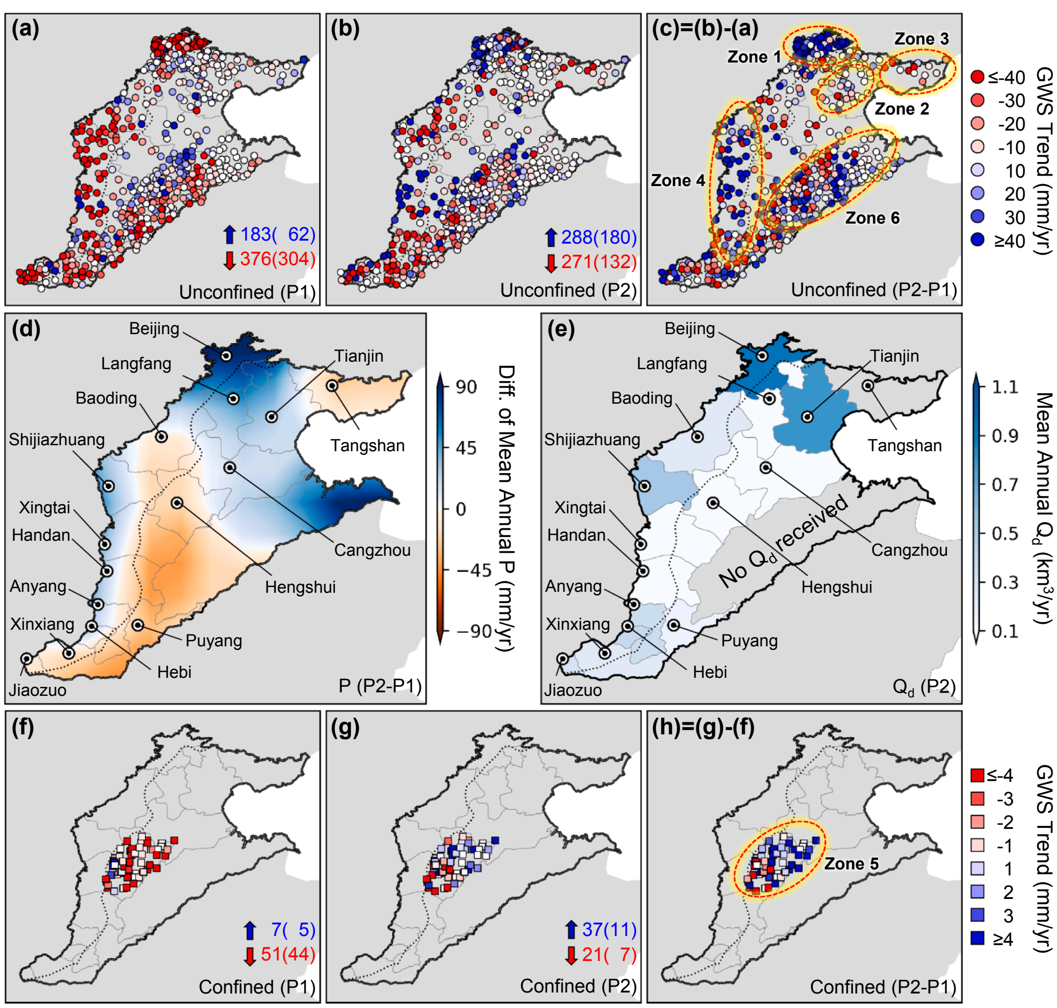

Fig. 3. Spatial distributions of GWS trends observed by the unconfined and confined wells during (a, f) P1 and (b, g) P2, as well as (c, h) their difference between two periods. (d) The difference of mean annual P and (e) the mean Q_d allocated to each city are also plotted. Blue (red) symbols represent the wells with an increasing (decreasing) GWS trend. The numbers in the parenthesis are the numbers of wells with a statistically significant GWS trend. Six zones in NCP are circled for detailed discussion.

considered negligible in NCP given that the large-sized surface water bodies are rare and ~40% of river channels are perennial dry in NCP regions (Wang et al., 2018; Gong et al., 2018). An independent estimation of the monthly GWS changes during 2003–2018 was derived by subtracting the sum of CLM-simulated SWE, CWS and SMS from GRACE TWS. Annual trends of GWS estimates (from well observations and GRACE data decomposition) during P1 and P2 are determined by using the non-parametric Mann-Kendall test (Kendall, 1975) with the confidence level of 95%.

2.3. Precipitation, MRP water diversion, and GW pumping data

The monthly precipitation (P) data during 2003–2018 were obtained from the gridded (0.5°) product from the China Meteorological Administration, which was produced from the interpolation of 2472 rain gauges records in China (Zhao and Zhu, 2015). Annual MRP-diverted water (Q_d) data during P2 and GW pumping (Q_p) data at each city (Fig. 1a) during P1 and P2 were collected from the official water resources bulletins annually published by Chinese government (BWA, 2018; TWA, 2018; HBWCD, 2018; HNWCD, 2018; HRWCC, 2018). The detailed data of Q_d and Q_p were listed respectively in Tables S1 and S2 in the supplementary material.

3. Results and discussion

3.1. Sub-regional GWS recovery from well observation

Fig. 3 plots the GWS trends during P1 and P2 at each of the 559 unconfined (Fig. 3a, b) and 58 confined (Fig. 3f, g) wells. To precisely identify the wells with GWS recovery, the difference in GWS trends of each period is plotted in Fig. 3c and h. The difference in mean annual P of two periods and the mean annual Q_d allocated to each city during P2 are plotted in Fig. 3d and e, respectively. In the following paragraphs, we evaluate the spatial pattern of GWS changes throughout the NCP first, and then identify 6 Zones to analyse the response of sub-regional GWS to P and Q_d changes separately.

For the 559 unconfined wells in NCP (Fig. 3a), GWS showed a decreasing trend during P1 in 376 (67%) wells with 304 (54%) statistically significant, while the rest 183 wells showed an increasing trend with only 62 significant. During P2 (Fig. 3b), however, GWS showed a decreasing trend in only 271 (48%) wells with 132 statistically significant, while the rest 288 (52%) wells showed an increasing trend with 180 statistically significant. For the 58 confined wells (Fig. 3f), GWS during P1 showed a decreasing trend in 51 (88%) wells with 44 significant, while the rest 7 wells showed an increasing trend with 5 significant. During P2 (Fig. 3g), however, GWS showed a decreasing trend in only 21 (36%) wells with 7 significant, while the rest 37 (64%) wells showed an increasing trend with 11 significant. These statistics show that the number of wells observing an increasing GWS trend during P2 was significantly more than that during P1, indicating the emergence of GWS recovery in NCP.

For the Zone 1 in Fig. 3c, GWS in most of the 87 unconfined wells near Beijing showed significant recovery (>30 mm/yr) in trend (i.e., P2 relative to P1), likely attributed to both 8% (47.5 mm/yr) increase of P (Fig. 3d) and 0.6 km^3/yr decrease of Q_p in P2 (Table S2). Mean Q_d during P2 was estimated at ~1.1 km^3/yr based on that $Q_d = 4.2$ km^3/yr for NCP and its allocation ratio to Beijing is ~24.8% (Table S1). There was also evidence of the increasing use (~0.05 km^3/yr) of recycled water and the managed aquifer recharge (~0.1 km^3/yr) in Beijing (BWA, 2018; Rogers et al., 2020). As noted by He et al. (2019), GW levels in parts of Beijing rose by 9 m and 11 m respectively in the unconfined and confined aquifers during 2014–2017. Long et al. (2020) stated that the mean absolute depth of GW level in the Beijing Plain had decreased by 3 m during 2014–2019. Our estimates agree well with these findings in that GWS in Beijing has started to recover as benefit from the increased recharge related to P surplus and the decreased Q_p after MRP operation (He et al., 2019; Long et al., 2020; Zhang et al., 2020b).

For the Zone 2 near Tianjin where P was increased by 24.1 mm/yr (4.7%) during P2 (Fig. 3d), weak GWS trends of <10 mm/yr were observed for both periods (Fig. 3a, b). This zone received 0.8 km^3/yr of Q_d (20.0% of the total 4.2 km^3/yr, the second largest next to Beijing in terms of MRP water received shown in Table S1), and mean Q_p after MRP operation was decreased by 0.174 km^3/yr (Table S2). Most of Q_d received near Tianjin were used to replace Q_p from the confined aquifers (Shang et al., 2016; Deng et al., 2018), explaining the lack of notable trends in the unconfined wells in this zone (Fig. 3b). The maximum confined GW depth at the cones of depression was decreased from 99.1 m in 2014 to 93.3 m in 2018 (TWA, 2018). Similar to Tianjin, several unconfined GWS near Tangshan (Zone 3 in Fig. 3c) showed higher depletion during P2 (>30 mm/yr, Fig. 3b), mainly reflecting the decreasing P (−11.8 mm/yr, Fig. 3d) since mean Q_p was decreased slightly by ~0.2 km^3/yr from 2009 to 2015 (same as Tianjin, Table S2).

The Zone 4, located near Shijiazhuang, Xingtai and Handan showed marked GWS recovery in the unconfined wells during P2 (~40 mm/yr, Fig. 3b). Shijiazhuang has the deepest cone of depression in the unconfined aquifers in NCP with the maximum depth over 60 m (Fig. S1). This area received ~0.5 km^3/yr of Q_d, the third largest next to Beijing and Tianjin, also a 22.4 mm/yr increase in P during P2 (Fig. 3d, e). Due to these two favourable factors, an alleviated GWS depletion trend was observed during P2 in Shijiazhuang, consistent with the Shu et al. (2012) and Ye et al. (2014) who found that the decreasing GWS trend cannot be completely reversed by Q_d in heavily irrigated areas. Xingtai and Handan are the key areas for implementing the shutdown of private wells (Shang et al., 2016). In two cities Q_p was reduced by > 50% (Table S2), while only 0.1 km^3/yr of Q_d were received (Fig. 3e). These cities are also among the subregions with the deepest cone of depression in unconfined aquifers in NCP (Fig. S1). The aquifers here are mainly recharged by the lateral inflow from west-bordering Taihang Mountain rather than recharge from P (Kendy et al., 2004; Cao et al., 2013), which explains that a few wells near the mountains observed the increasing GWS trends (Fig. 3b, d).

For the deeper confined wells in Zone 5 (Fig. 3h), the largest cone of depression over NCP with the maximum depth of >100 m occurred near Hengshui (Fig. S1). The confined GWS in this zone was depleted significantly during P1, with the rate of −3 mm/yr. Interestingly, although the mean annual P was decreased by 14.2 mm/yr (Fig. 3d) and only received 0.1 km^3/yr of Q_d during P2 (Fig. 3e), GWS in the confined wells showed a significant increasing trend (~4 mm/yr) (Fig. 3g, h). Since Q_d is too small to cause substantial reduction in Q_p (Table S2) and P was decreased during P2 (Fig. 3d), the significant GWS recovery in the confined wells can mainly be attributed to the implementation of management measures such as the shutdown of most private wells to curtail Q_p in Hengshui and Cangzhou, as reported by Shang et al. (2016). For other confined wells located in Xingtai where less regulatory measures were implemented, GWS trend only reflects the trend of P (Fig. 3d, h).

The Zone 6 (Fig. 3c, e) located in the Shandong Province is not belonging to the water-receiving area of MRP. However, this zone received the diverted water from the eastern route of the South-to-North water diversion project (Yao et al., 2019), which began its operation in November 2013. By 2019 it has received 4.0 km^3/yr of diverted water and hence Q_p was reduced in this zone (Yao et al., 2019). The mean P during P2 was decreased by 34.2 mm/yr in the southwest part and increased by 37.8 mm/yr in the northeast part (Fig. 3d), overall in consistency with the spatial patterns that the unconfined wells in the north-eastern Zone 6 with the milder GWS trends than those in the south-western part (Fig. 3b). Determining the effect of the eastern route project is beyond the scope of current study, so no much explanation is available here.

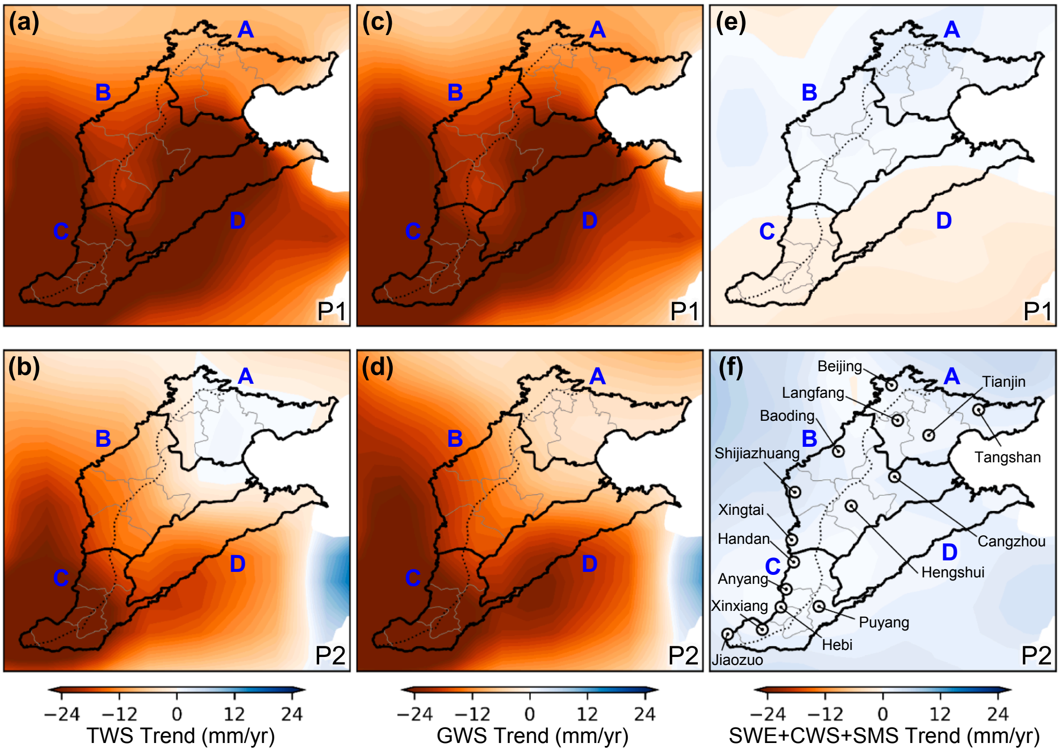

Fig. 4. Annual trend maps of (a, b) GRACE-estimated TWS, (c, d) GWS, and (e, f) CLM-simulated SMS during (a, c, e) P1 and (b, d, f) P2 in NCP. By referring to the spatial pattern of GWS changes in Fig. 4d and the well observations in Fig. 3c, the NCP is divided into four subregions that are numbered by A, B, C, and D, respectively. The same city names as those in Fig. 3e are marked in Fig. 4f. All the trend maps were spatially smoothed by 150-km-radius Gaussian filter for the purpose of better visualization.

3.2. GRACE estimation of sub-regional GWS recovery

As an independent estimate, Fig. 4 plots the spatial distributions of the trends of GRACE-estimated TWS and GWS, as well as the sum of CLM-simulated SWE, CWS and SMS during P1 and P2. On average, the trend magnitude in the sum of SWE, CWS and SMS (+1.2 mm/yr, Fig. 4e, f) only accounts for ~5% of TWS trend (−26.1 mm/yr, Fig. 4a, b) in NCP. High consistency between TWS and GWS trends can be observed (grid-to-grid correlation $R > 0.93$, Fig. 4a–d) for both periods, indicating the dominant role of GWS on TWS. The finding is consistent with most previous studies related to TWS component decomposition in NCP (e.g., Feng et al., 2013; Huang et al., 2015; Pan et al., 2017; Rodell et al., 2018).

A decreasing trend of GWS (−24.7 mm/yr) was found over NCP during P1 (Fig. 4c), smaller than previous estimate of −32.0 mm/yr (2003–2013) by Huang et al. (2015), but larger than −22.0 mm/yr (2003–2010) by Feng et al. (2013), −17.1 mm/yr (2005–2013) by Gong et al. (2018), and −17.0 mm/yr (2004–2016) by Zhao et al. (2019). The discrepancy is to a large extent due to different study periods, GRACE data and processing methods used. The spatial patterns agree well with that of well observations (Fig. 3a vs. Fig. 4c), also similar with Rodell et al. (2018, Fig. 1) showing significant GWS depletion in NCP.

During P2, GRACE-estimated GWS showed a mild recovery in regions near Beijing (Fig. 4d). Although the estimated trend of GWS recovery is small (~1.0 mm/yr), the spatial location corresponds well to that of well-observed GWS recovery shown in Fig. 3b. We note that the scale of GWS recovery is smaller than the spatial resolution of GRACE data (300 km × 300 km ≈ 100,000 km^2, Watkins et al., 2015), making the interpretation of GRACE estimates rather difficult (Longuevergne et al., 2013; Save et al., 2016; Yeh et al., 2006). Nevertheless, the GRACE-derived spatial pattern of GWS trend provides a reference to divide the NCP into four sub-regions as shown in Fig. 4: Subregions A (35,500 km^2), B (47,900 km^2), C (24,400 km^2) and D (32,200 km^2). The boundaries of each subregion are determined jointly by the spatial patterns of GWS changes detected by GRACE and well observations, as well as the boundaries of cities that received Q_d within NCP. Such partition is actually difficult to achieve if only analysing the spatial pattern of GWS changes observed by in-situ wells, as shown in Fig. 3. For further investigation, the quantitative statistics of the estimated GWS trends from in-situ wells and GRACE data in each subregion are summarized in Table 1. The details will be discussed in the next section.

3.3. Quantitative analysis of sub-regional GWS recovery

Fig. 5a plots the monthly GWS changes from wells and GRACE in NCP during 2003–2018. GWS estimated from wells showed a decreasing trend of −19.1 ± 5.1 mm/yr, while GRACE estimate showed a −24.7 ± 8.0 mm/yr decrease during P1 (Table 1). During P2, however, GWS estimate from wells showed an increasing trend of +1.8 ± 0.7 mm/yr while GRACE estimate indicated a decrease of −16.6 ± 4.7 mm/yr. R and RMSE between two estimates are 0.88 and 62.5 mm, respectively (Fig. 5a). The large RMSE is due to the small seasonal amplitude of GRACE GWS versus well observations, mainly caused by that (1) sub-regional GRACE data are contaminated by the signal leakage and amplitude-damping effects (Feng et al., 2013; Huang et al., 2015); (2) the over-estimated specific yield (storage coefficient) is used in converting GW level to GWS. During P1 and P2, GWS trend in the unconfined wells is −16.4 ± 3.6 and +1.4 ± 0.5 mm/yr, respectively, significantly larger than that in the confined wells of −2.6 ± 1.3 and +0.4 ± 0.1 mm/yr, indicating the predominant role of unconfined aquifers in NCP in GWS depletion and recovery (Table 1) given that the magnitude of specific yields (0.025 ~ 0.290) used is 2 ~ 3 orders of magnitude larger than the storage coefficient (0.0004 ~ 0.0045) in NCP.

Fig. 5b compares the monthly GWS estimates from wells and GRACE in PP and ECP during 2003–2018. For PP and ECP, R (RMSE) between two GWS estimates are 0.92 (72.3 mm) and 0.69 (117.0 mm),

Table 1
Statistics of the GWS trends (unit: mm/yr) estimated by in-situ wells and GRACE data during 2003–2014 and 2015–2018 in NCP, PP, ECP, and four subregions (A, B, C and D). GWS trends in the unconfined and confined wells are given separately. "*" highlights that the GWS trend is insignificant at the confidence level of 95%.

Variable	NCP		PP		ECP		A		B		C		D	
	03–14	15–18	03–14	15–18	03–14	15–18	03–14	15–18	03–14	15–18	03–14	15–18	03–14	15–18
GWS In-situ	−19.1 ± 5.1	1.8 ± 0.7*	−34.3 ± 4.7	4.9 ± 1.3*	−2.0 ± 1.5*	−3.6 ± 1.1*	−15.8 ± 2.6	7.7 ± 1.8*	−13.9 ± 3.2	−5.4 ± 1.1*	−28.4 ± 4.4	−7.8 ± 2.1*	2.8 ± 0.6*	11.2 ± 2.3
GWS GRACE	−24.7 ± 8.0	−16.6 ± 4.7	−22.5 ± 6.9	−18.2 ± 6.8	−25.0 ± 5.9	−15.3 ± 4.4	−16.1 ± 5.8	1.2 ± 0.7*	−22.3 ± 5.8	−11.4 ± 4.3	−29.5 ± 7.9	−26.2 ± 7.4	−26.6 ± 6.8	−17.0 ± 5.7*
GWS Unconfined	−16.4 ± 3.6	1.4 ± 0.5*	−34.3 ± 4.7	4.9 ± 1.3*	0.6 ± 0.2*	−4.0 ± 1.0*	−15.8 ± 2.6	7.7 ± 1.8*	−11.3 ± 2.0	−5.8 ± 1.0*	−28.4 ± 4.4	−7.8 ± 2.1*	2.8 ± 0.6*	11.2 ± 2.3
GWS Confined	−2.6 ± 1.3*	0.4 ± 0.1*			−2.6 ± 1.3*	0.4 ± 0.1*			−2.6 ± 1.3*	0.4 ± 0.1*				

respectively. The increase in RMSE relative to that in NCP (62.5 mm) is likely associated with the accuracy of GRACE data decreasing with the size of study area. GWS trends during P1 and P2 from well observations were −34.3 ± 4.7 and +4.9 ± 1.3 mm/yr for PP and −2.0 ± 1.5 and −3.6 ± 1.1 mm/yr for ECP, whereas that estimated from GRACE were −22.5 ± 6.9 and −18.2 ± 6.8 mm/yr for PP and −25.0 ± 5.9 and −15.3 ± 4.4 mm/yr for ECP (Table 1). Well observations show that GWS variability in PP is considerably larger than that in ECP, but GRACE may have difficulty to distinguish the respective signals in two subregions even with the use of the scale factors to reduce leakage errors. The GWS recovery signals in PP may be offset by the leakage of GWS depletion signals from ECP and surrounding areas outside NCP (Fig. 3d). Similarly, some signals from PP may interfere GRACE detection of GWS trend in ECP (Huang et al., 2015).

Fig. 5c compares the 2003–2018 monthly GWS estimates from wells and GRACE in four subregions, with the corresponding R (RMSE) between them 0.73 (78.9 mm), 0.85 (79.2 mm), 0.90 (80.6 mm) and 0.65 (166.5 mm) in subregions A, B, C and D, respectively. The largest GWS depletion trend during P1 estimated from wells (−28.4 ± 4.4 mm/yr) or GRACE (−29.5 ± 7.9 mm/yr) occurred in subregion C. The GWS trend estimated from GRACE (−16.1 ± 5.8 mm/yr) in subregion A is close to that from well observations (−15.8 ± 2.6 mm/yr), while GRACE (−22.3 ± 5.8 mm/yr) tends to overestimate the GWS depletion trend in subregion B relative to well observations (−13.9 ± 3.2 mm/yr) (Table 1). GRACE estimated a large GWS depletion trend (−26.6 ± 6.8 mm/yr) in subregion D where well observations estimated a lack of trend (+2.8 ± 0.6 mm/yr). The inconsistent or even opposite GWS trends from well observations and GRACE estimates further illustrate that the leakage errors may still present to interfere the GRACE estimates of GWS depletion in four subregions.

During P2, GWS in subregions A and D showed an increasing trend of +7.7 ± 1.8 and +11.2 ± 2.3 mm/yr respectively from well observations, but those estimated from GRACE were +1.2 ± 0.7 and −17.0 ± 5.7 mm/yr, respectively. For subregions B and C, GWS trends from well observations were −5.4 ± 1.1 and −7.8 ± 2.1 mm/yr, respectively, whereas that estimated from GRACE were −11.4 ± 4.3 and −26.2 ± 7.4 mm/yr (Table 1). This is interesting because GRACE detected the small trend of GWS recovery in subregion A, but was unable to detect the large trend of GWS recovery in subregion D. The main reason for this is that GRACE has the potential to detect the signal within a smaller area if the mass change is highly concentrated and with a sufficiently large magnitude (Longuevergne et al., 2013). Existing studies have successfully applied GRACE data to detect reservoir water impoundment, ice melting and groundwater depletion in areas as small as 400 km^2 (e.g., Chen et al., 2007; Famiglietti et al., 2011; Wang et al., 2011; Yi et al., 2017). According to the well observations shown in Fig. 3b, the GWS recovery in NCP is likewise highly concentrated in subregion A (i.e., Beijing), which is intrinsically similar to the reservoir water impoundment but occurring below the land surface. Hence it is reasonable to anticipate that GRACE may have the potential to detect the sub-regional GWS recovery in NCP, but not yet able to estimate the magnitude accurately due to the signal leakage.

3.4. Uncertainty estimation

The monthly errors of GWS estimation from well observations (shown as the pink envelopes in Fig. 5) were quantified by assuming a ±20% uncertainty of the specific yield and storage coefficient by referring to the studies of Huang et al. (2015) and Pan et al. (2017). The errors of GRACE GWS (shown as green envelopes in Fig. 5) were calculated by propagating the errors of GRACE TWS and CLM-simulated SMS, SWE and CWS. The error of GRACE TWS was derived by considering the calibration error as provided in GRACE JPL mascon solution (Watkins et al., 2015; Wiese et al., 2018). The leakage errors were not considered herein because the scale factors were used for calibrate GRACE TWS prior to the uncertainty estimation. This may

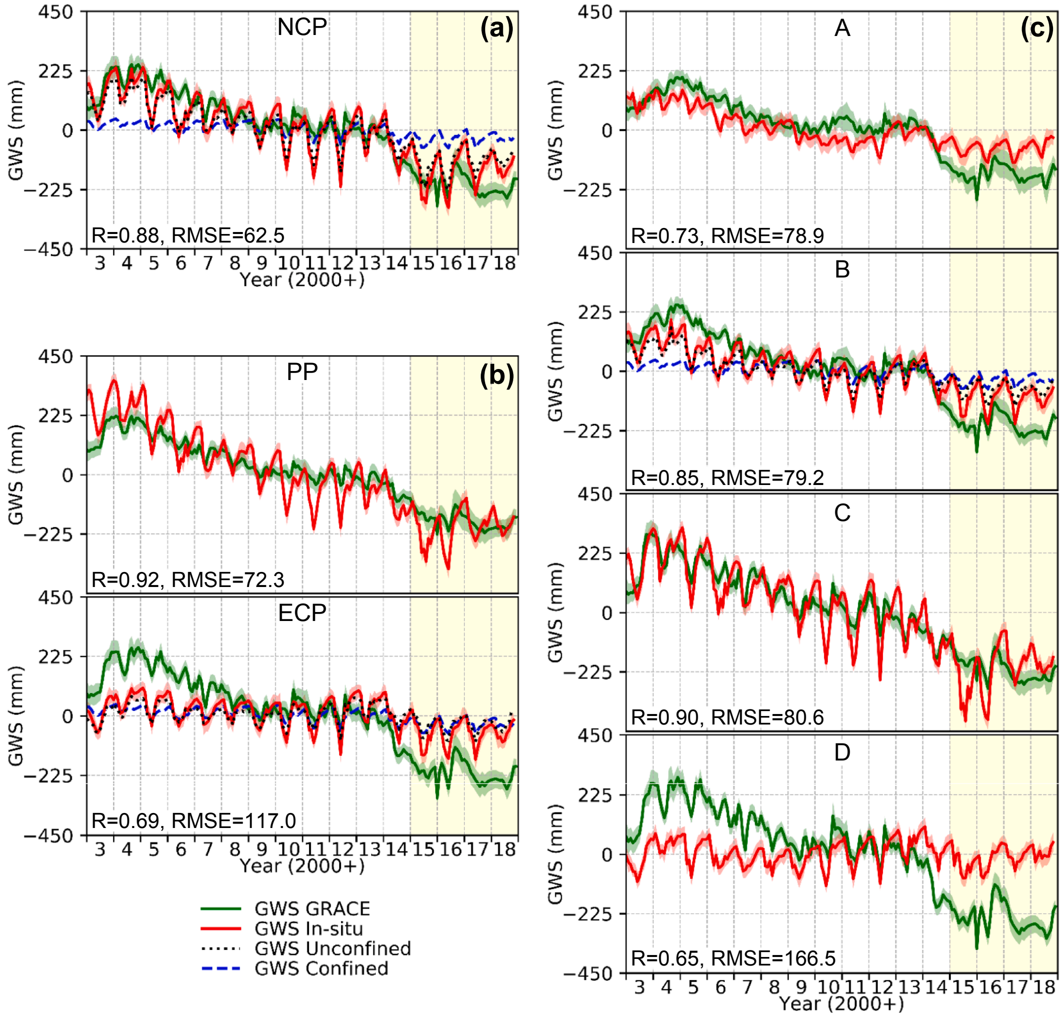

Fig. 5. Comparisons of monthly GWS from well observations and GRACE estimation during 2003-2018 in (a) NCP, (b) PP and ECP, and (c) four subregions (A, B, C, and D shown in Fig. 4), with the corresponding correlation coefficient (R) and root-mean-square error (RMSE, mm) given. GWS estimates from the unconfined and confined wells are plotted separately. The pink and green envelopes represent the uncertainties of well observations and GRACE estimation, as will be discussed in Section 3.4.

underestimate the error of TWS if the scale factors used cannot eliminate the leakage errors completely. CLM does not provide the error estimation for the simulated variables. Hence the errors of SMS, SWE and CWS was calculated as one standard deviation of the simulations from four GLDAS models (Pan et al., 2017).

Table 2 summarizes the estimated monthly mean errors of TWS and its components in NCP, PP, ECP and four subregions. As seen, the errors of in-situ observed GWS range 13.1 ~ 19.8 mm/month in NCP and its subregions. GWS in ECP has the highest error, implying a highly uneven changes of GWS within subregion. The errors of GRACE GWS range 31.3 ~ 39.1 mm/month, dominated by GRACE TWS errors (30.2 ~ 37.7 mm/month) and followed by the errors of three CLM-simulated water storage components (8.1 ~ 12.0 mm/month). By comparison, the error of GWS estimated by GRACE data is about two times larger than that estimated by well observations (Table 2). This hints that the in-situ GW measurements by in-situ wells will be indispensable for monitoring GWS recovery in NCP.

Table 2
Summary of the monthly errors (unit: mm) of in-situ observed GWS, GRACE TWS, CLM-simulated SMS, SWE, and CWS, and GRACE-estimated GWS in NCP, PP, ECP, and four subregions (A, B, C and D).

Variable	NCP	PP	ECP	A	B	C	D
GWS In-situ	17.2	13.1	19.8	15.0	13.9	18.8	16.1
TWS GRACE	33.3	36.7	31.5	37.7	30.2	33.8	37.3
SMS + SWE + CWS CLM	9.7	8.1	11.1	9.0	8.2	12.0	11.7
GWS GRACE	34.7	37.6	33.4	38.8	31.3	35.9	39.1

4. Concluding remarks

This study addresses the important science question that whether MRP has contributed to GWS recovery in NCP since its MRP operation in December 2014. To this end, long-term GW level data from 617 monitoring wells (559 unconfined and 58 confined wells) in NCP were used to analyse the spatiotemporal variations of GWS before and after the MRP operation (i.e., the P1 period of 2003–2014 and P2 period of 2015–2018). The satellite-measured TWS data from GRACE and GRACE-FO were also used in conjunction with model simulations to estimate GWS in NCP and four sub-regions, providing an independent validation against the well-based observational GWS estimates particularly on the sub-regional spatial patterns. The main causes for observed sub-regional GWS depletion (P1) and recovery (P2) were investigated through the analyses of precipitation (P), pumping (Q_p), and MRP-diverted water (Q_d) data at each of 14 cities along the MRP conveyance route.

For the entire NCP, GWS estimate from well observations showed a −19.1 ± 5.1 mm/yr of decreasing trend during P1, compared to that from GRACE of -24.7 ± 8.0 mm/yr. However, GWS estimate from wells showed a $+1.8 \pm 0.7$ mm/yr of increasing trend during P2, in contrast to the estimate from GRACE of -16.6 ± 4.7 mm/yr. Sub-regional GWS recovery in NCP can be observed from well data in water-receiving cities along the MRP conveyance route, also in consistency with the received MRP water and pumping reduction data in each city. GWS depletion of -34.3 ± 4.7 mm/yr during P1 and recovery of $+4.9 \pm 1.3$ mm/yr during P2 occur mainly in the unconfined aquifers of PP, which are considerably larger than -2.0 ± 1.5 and -3.6 ± 1.1 mm/yr in ECP. Yet GRACE is difficult to distinguish the respective signals in PP and ECP due to signal leakage.

The following specific findings at the sub-regional scales can be summarized from this study:

1. For the total 617 wells, 67% (88%) of the unconfined (confined) wells had decreasing trends during P1, while the numbers decreasing to only 48% (36%) during P2, indicating GWS recovery occurred in both unconfined and confined GWS in NCP after MRP operation.
2. Significant GWS recovery (>30 mm/yr) was observed in most of the 87 wells (all unconfined) near Beijing attributed to both +8% of increase in P and +0.6 km^3/yr decrease in Q_p due to received MRP Q_d (1.1 km^3/yr, 22.4% of total Q_d diverted to NCP) during P2.
3. Significant GWS recovery (>20 mm/yr) was observed in 25 unconfined wells at the agricultural regions near Shijiazhuang, Xingtai and Handan, attributed to the decreasing Q_p, increasing P, and likely the resulting increase in lateral inflow recharge from west-bordering Taihang Mountain.
4. GWS recovery in the confined aquifers (~4 mm/yr) was found in Hengshui due specifically to the 20% decrease in Q_p as the result of recent policy enforcement of well shutdown, since Q_d was as small as +0.1 km^3/yr and P was decreased by −13%.
5. GRACE indeed has the potential to locate GWS depletion and recovery hotspots at the sub-regional scales of NCP smaller than the spatial resolution (100,000 km^2), but with considerable leakage errors interfering the accuracy of estimated variability and trend magnitude.

This study highlights that GWS in NCP has started a gradual transition from depletion to recovery in the major water-receiving areas of the MRP water diversion, but it remains to be observed and investigated whether the trend will be reversed again under future more frequent drought occurrence.

CRediT authorship contribution statement

Chong Zhang: Visualization, Writing - original draft, Funding acquisition. **Qingyun Duan:** Writing - review & editing, Funding acquisition. **Pat J.-F. Yeh:** Writing - review & editing. **Yun Pan:** Writing - review & editing, Funding acquisition. **Huili Gong:** Investigation. **Hamid Moradkhani:** Investigation. **Wei Gong:** Investigation. **Xiaohui Lei:** Resources. **Weihong Liao:** Data curation. **Lei Xu:** Software. **Zhiyong Huang:** Methodology. **Longqun Zheng:** Visualization. **Xueru Guo:** Visualization.

Declaration of Competing Interest

The authors declare that they have no known competing financial interests or personal relationships that could have appeared to influence the work reported in this paper.

Acknowledgments

This study was jointly supported by the Strategic Priority Research Program of the Chinese Academy of Sciences (XDA20060401), the National Natural Science Foundation of China (51979004, 41622101, 41877155, and 41771456), and the China Scholarship Council (201906040156). The groundwater level data are publicly available on the Data Sharing Repository of National Earth System Science Data Center (https://www.doi.org/10.12041/geodata.10392011028646.ver1.db). The data of GLDAS simulation and GRACE (Follow-on) solution are provided by the official data sharing repositories maintained by NASA (https://ldas.gsfc.nasa.gov/gldas) and JPL (https://grace.jpl.nasa.gov/data/get-data/jpl_global_mascons/), respectively. We thank these institutes who provided data for this study. We also thank the anonymous reviewers and editors for their constructive comments.

Appendix A. Supplementary data

Supplementary data to this article can be found online at https://doi.org/10.1016/j.jhydrol.2021.126156.

References

Beijing Water Authority (BWA), 2018. Annual bulletin of water resources in Beijing municipality. [Available at: http://swj.beijing.gov.cn/].
Cao, G., Zheng, C., Scanlon, B.R., Liu, J., Li, W., 2013. Use of flow modeling to assess sustainability of groundwater resources in the North China Plain. Water Resour. Res. 49 (1), 159–175. https://doi.org/10.1029/2012WR011899.
Chen, J.L., Wilson, C.R., Tapley, B.D., Blankenship, D.D., Ivins, E.R., 2007. Patagonia Icefield melting observed by Gravity Recovery and Climate Experiment (GRACE). Geophys. Res. Lett. 34 (22), L22501. https://doi.org/10.1029/2007GL031871.
Cleveland, R., Cleveland, W., McRae, J., Terpenning, I., 1990. STL: A seasonal trend decomposition procedure based on loess. J. Off. Stat. 6, 3–73.
Deng, X., Li, F., Zhao, Y., Li, S., 2018. Regulation of deep groundwater based on MODFLOW in the water intake area of the south-to-north water transfer project in Tianjin. China. J. Hydroinfo. 20 (4), 989–1007. https://doi.org/10.2166/hydro.2018.126.
Famiglietti, J.S., 2014. The global groundwater crisis. Nat. Clim. Change. 4 (11), 945–948. https://doi.org/10.1038/nclimate2425.
Famiglietti, J.S., Lo, M., Ho, S.L., Bethune, J., Anderson, K.J., Syed, T.H., Swenson, S.C., de Linage, C.R., Rodell, M., 2011. Satellites measure recent rates of groundwater depletion in California's Central Valley. Geophys. Res. Lett. 38 (3), L03403. https://doi.org/10.1029/2010GL046442.
Feng, W., Shum, C., Zhong, M., Pan, Y., 2018. Groundwater storage changes in China from satellite gravity: An overview. Remote Sens. 10 (5), 674. https://doi.org/10.3390/rs10050674.
Feng, W., Zhong, M., Lemoine, J.M., Biancale, R., Hsu, H.T., Xia, J., 2013. Evaluation of groundwater depletion in North China using the Gravity Recovery and Climate Experiment (GRACE) data and ground-based measurements. Water Resour. Res. 49 (4), 2110–2118. https://doi.org/10.1002/wrcr.20192.
Foster, S., Garduno, H., Evans, R., Olson, D., Tian, Y., Zhang, W., Han, Z., 2004. Quaternary aquifer of the North China Plain-Assessing and achieving groundwater resource sustainability. Hydrogeol. J. 12 (1), 81–93. https://doi.org/10.1007/s10040-003-0300-6.
Fritsch, F.N., Carlson, R.E., 1980. Monotone piecewise cubic interpolation. SIAM J. Numer. Anal. 17 (2), 238–246. https://doi.org/10.1137/0717021.
Gao, Y., Li, J., Hao, Q., Yu, C., Meng, S., 2018. Analysis on the effect of groundwater overexploitation control in water receiving region of the first phase of the south-north water transfer project. MATEC Web of Conferences 246. https://doi.org/10.1051/matecconf/201824601069.
Gong, H., Pan, Y., Zheng, L., Li, X., Zhu, L., Zhang, C., Huang, Z., Li, Z., Wang, H., Zhou C., 2018. Long-term groundwater storage changes and land subsidence development in the North China Plain (1971–2015). Hydrogeol. J. 26, 1417–1427. https://doi.org/10.1007/s10040-018-1768-4.
Haihe River Water Conservancy Commission (HRWCC), 2018. Annual bulletin of water resources in Haihe River basin. [Available at: http://www.hwcc.gov.cn/].
He, Y., Li, S., Li, Y., Meng, X., Liu, C., 2019. Effect of South-to-North water transfer project on recharge and water level in Chaobai river area (in Chinese). Beijing Water 3, 21–26.
Hebei Water Conservancy Department (HBWCD), 2018. Annual bulletin of water resources in Hebei province. [Available at: http://slt.hebei.gov.cn/].
Henan Water Conservancy Department (HNWCD), 2018. Annual bulletin of water resources in Henan province. [Available at: http://www.hnsl.gov.cn/].
Huang, Z., Pan, Y., Gong, H., Yeh, P.-F., Li, X., Zhou, D., Zhao, W., 2015. Sub-regional-scale groundwater depletion detected by GRACE for both shallow and deep aquifers in North China Plain. Geophys. Res. Lett. 42 (6), 1791–1799. https://doi.org/10.1002/grl.v42.610.1002/2014GL062498.
Institute of China Geological Environment Monitoring (ICGEM), 2018. China Geological Environment Monitoring: Groundwater Yearbook (in Chinese). Vastplain House, Beijing.
Kendall, M.G., 1975. Rank correlation methods. Griffin, London.
Kendy, E., Zhang, Y., Liu, C., Wang, J., Steenhuis, T., 2004. Groundwater recharge from irrigated cropland in the North China Plain: Case study of Luancheng County, Hebei Province, 1949–2000. Hydrol. Process. 18 (12), 2289–2302. https://doi.org/10.1002/(ISSN)1099-108510.1002/hyp.v18:1210.1002/hyp.5529.
Landerer, F. W., Flechtner, F. M., Save, H., Webb, F. H., Bandikova, T., Bertiger, W. I., et al. 2020. Extending the global mass change data record: GRACE Follow-On

instrument and science data performance. Geophys. Res. Lett. 47, e2020GL088306. https://doi.org/10.1029/2020GL088306.

Lei, X., Zheng, H., Shang, Y., Wang, H., 2018. Assessing emergency regulation technology in the Middle Route of the South-to-North Water Diversion Project. China. Int. J. Water Resour. D. 34 (3), 405–417. https://doi.org/10.1080/07900627.2018.1441707.

Liu, C., Xia, J., 2004. Water problems and hydrological research in the Yellow River and the Huai and Hai River basins of China. Hydrol. Process. 18 (12), 2197–2210. https://doi.org/10.1002/(ISSN)1099-108510.1002/hyp.v18:1210.1002/hyp.5524.

Liu, C., Yu, J.J., Kendy, E., 2001. Groundwater exploitation and its impact on the environment in the North China Plain. Water Inter. 26 (2), 265–272. https://doi.org/10.1080/02508060108686913.

Liu, C., Zheng, H., 2002. South-to-north Water Transfer Schemes for China. Int. J. Water Resour. D 18 (3), 453–471. https://doi.org/10.1080/0790062022000006934.

Liu, J., Zheng, C., Zheng, L., Lei, Y., 2008. Ground water sustainability: Methodology and application to the North China Plain. Groundwater 46 (2), 897–909. https://doi.org/10.1111/j.1745-6584.2008.00486.x.

Long, D., Yang, W., Scanlon, B.R., Zhao, J., Liu, D., Burek, P., et al., 2020. South-to-North Water Diversion stabilizing Beijing's groundwater levels. Nat. Commun. 11 (12), 3665. https://doi.org/10.1038/s41467-020-17428-6.

Longuevergne, L., Wilson, C.R., Scanlon, B.R., Crétaux, J.F., 2013. GRACE water storage estimates for the Middle East and other regions with significant reservoir and lake storage. Hydrol. Earth Syst. Sci. 17 (12), 4817–4830. https://doi.org/10.5194/hess-17-4817-2013.

Pan, Y., Zhang, C., Gong, H., Yeh, P.J.F., Shen, Y., Guo, Y., Huang, Z., Li, X., 2017. Detection of human-induced evapotranspiration using GRACE satellite observations in the Haihe River basin of China. Geophys. Res. Lett. 44 (1), 190–199. https://doi.org/10.1002/2016GL071287.

Rodell, M., et al., 2004. The Global Land Data Assimilation System. Bull. Amer. Meteor. Soc. 85 (3), 381–394. https://doi.org/10.1175/BAMS-85-3-381.

Rodell, M., Famiglietti, J.S., Wiese, D.N., Reager, J.T., Beaudoing, H.K., Landerer, F.W., Lo, M.-H., 2018. Emerging trends in global freshwater availability. Nat. Analy. 557, 651–659. https://doi.org/10.1038/s41586-018-0123-1.

Rogers, S., Chen, D., Jiang, H., Rutherfurd, I., Wang, M., Webber, M., Crow-Miller, B., Barnett, J., Finlayson, B., Jiang, M., Shi, C., Zhang, W., 2020. An integrated assessment of China's South-North Water Transfer Project. Geogr. Res. 58 (1), 49–63. https://doi.org/10.1111/geor.v58.110.1111/1745-5871.12361.

Save, H., Bettadpur, S., Tapley, B.D., 2016. High resolution CSR GRACE RL05 mascons. J. Geophys. Res. 121 (10), 7547–7569. https://doi.org/10.1002/2016JB013007.

Shang, Y., You, B., Shang, L., 2016. China's environmental strategy towards reducing deep groundwater exploitation. Environ. Earth Sci. 75, 1439. https://doi.org/10.1007/s12665-016-6110-7.

Shao, J.L., Li, L., Cui, Y.L., Zhang, Z.L., 2013. Groundwater flow simulation and its Application in Groundwater Resource Evaluation in the North China Plain, China. Acta. Geol. Sin.-Engl. 87, 243–253. https://doi.org/10.1111/1755-6724.12045.

Shao, R., Zhang, B., Su, T., Long, B., Cheng, L., Xue, Y., Yang, W., 2019. Estimating the increase in regional evaporative water consumption as a result of vegetation restoration over the Loess Plateau. China. J. Geophys. Res. 124 (22), 11783–11802. https://doi.org/10.1029/2019jd031295.

Shu, Y., Villholth, K.G., Jensen, K.H., Stisen, S., Lei, Y., 2012. Integrated hydrological modeling of the North China Plain: options for sustainable groundwater use in the alluvial plain of Mt. Taihang. J. Hydrol. 464 (25), 79–93. https://doi.org/10.1016/j.jhydrol.2012.06.048.

Tianjin Water Authority (TWA), 2018. Annual bulletin of water resources in Tianjin municipality. [Available at: http://swj.tj.gov.cn/].

Wang, X., de Linage, C., Famiglietti, J., Zender, C.S., 2011. Gravity Recovery and Climate Experiment (GRACE) detection of water storage changes in the Three Gorges Reservoir of China and comparison with in situ measurements. Water Resour. Res. 47 (12), W12502. https://doi.org/10.1029/2011WR010534.

Wang, Y., Zheng, C., Ma, R., 2018. Review: Safe and sustainable groundwater supply in China. Hydrogeol. J. 26, 1301–1324. https://doi.org/10.1007/s10040-018-1795-1.

Watkins, M.M., Wiese, D.N., Yuan, D.N., Boening, C., Landerer, F.W., 2015. Improved methods for observing earth's time variable mass distribution with GRACE using spherical cap mascons. J. Geophys. Res. 120 (4), 2648–2671. https://doi.org/10.1002/2014JB011547.

Wiese, D.N., Landerer, F.W., Watkins, M.M., 2016. Quantifying and reducing leakage errors in the JPL RL05M GRACE mascon solution. Water Resour. Res. 52 (9), 7490–7502. https://doi.org/10.1002/2016WR019344.

Wiese, D.N., Yuan, D.N., Boening, C., Landerer, F.W., Watkins, M.M., 2018. JPL GRACE and GRACE-FO Mascon Ocean, Ice, and Hydrology Equivalent Water Height JPL Release 06 Version 02. Ver. 2. PO.DAAC, CA, USA, https://doi.org/10.5067/TEMSC-3MJ62. Dataset accessed [2021-01-15].

Xu, L., Chen, N., Zhang, X., Chen, Z., 2019. Spatiotemporal changes in China's terrestrial water storage from GRACE satellites and its possible drivers. J. Geophys. Res. 124 (22), 11976–11993. https://doi.org/10.1029/2019JD031147.

Yao, Y., Zheng, C., Andrews, C., He, X., Zhang, A., Liu, J., 2019. Integration of groundwater into China's south-north water transfer strategy. Sci. Total Environ. 658 (25), 550–557. https://doi.org/10.1016/j.scitotenv.2018.12.185.

Ye, A., Duan, Q., Chu, W., Xu, J., Mao, Y., 2014. The impact of the South-North Water Transfer Project (CTP)'s central route on groundwater table in the Hai River basin. North China. Hydrol. Process. 28 (23), 5755–5768. https://doi.org/10.1002/hyp.10081.

Yeh, P.J.F., Swenson, S.C., Famiglietti, J.S., Rodell, M., 2006. Remote sensing of groundwater storage changes in Illinois using the Gravity Recovery and Climate Experiment (GRACE). Water Resour. Res. 42 (12), W12203. https://doi.org/10.1029/2006WR005374.

Zhang, B., Xia, Y., Long, B., Hobbins, M., Zhao, X., Hain, C., Li, Y., Anderson, M.C., 2020a. Evaluation and comparison of multiple evapotranspiration data models over the contiguous United States: implications for the next phase of NLDAS (NLDAS-Testbed) development. Agricult. For. Meteorol. 280, 107810. https://doi.org/10.1016/j.agrformet.2019.107810.

Yi, S., Song, C., Wang, Q., Wang, L., Heki, K., Sun, W., 2017. The potential of GRACE gravimetry to detect the heavy rainfall-induced impoundment of a small reservoir in the upper Yellow River. Water Resour. Res. 53 (8), 6562–6578. https://doi.org/10.1002/2017WR020793.

Zhang, C., Duan, Q., Yeh, P.-F., Pan, Y., Gong, H., Gong, W., Di, Z., Lei, X., Liao, W., Huang, Z., Zheng, L., Guo, X., 2020b. The effectiveness of the South-to-North Water Diversion Middle Route Project on water delivery and groundwater recovery in North China Plain. Water Resour. Res. 56 (10) https://doi.org/10.1029/2019WR026759.

Zhang, M., Hu, L., Yao, L., Yin, W., 2018. Numerical studies on the influences of the South-to-North Water Transfer Project on groundwater level changes in the Beijing Plain, China. Hydrol. Process. 32 (12), 1858–1873. https://doi.org/10.1002/hyp.v32.1210.1002/hyp.13125.

Zhang, Z., Fei, Y., Chen, Z., et al., 2009. Survey and Evaluation of Ground-Water Sustainable Utilization in North China Plain (in Chinese). Geological House, Beijing.

Zhao, Y., Zhu, J., 2015. Assessing quality of grid daily precipitation datasets in China in recent 50 years (in Chinese). Plateau Meteorol. 34, 50–58.

Zheng, C., Liu, J., Cao, G., Kendy, E., Wang, H., Jia, Y., 2010. Can China cope with its water crisis? – Perspectives from the North China Plain. Groundwater 48 (3), 350–354. https://doi.org/10.1111/j.1745-6584.2010.00695_3.x.

Zheng, L., Pan, Y., Gong, H., Huang, Z., Zhang, C., 2020. Comparing Groundwater Storage Changes in Two Main Grain Producing Areas in China: Implications for Sustainable Agricultural Water Resources Management. Remote Sens. 12 (13), 1–21. https://doi.org/10.3390/rs12132151.

Zhou, F., Bo, Y., Ciais, P., Dumas, P., Tang, Q., Wang, X., Liu, J., Zheng, C., Polcher, J., Yin, Z., Guimberteau, M., Peng, S., Ottle, C., Zhao, X., Zhao, J., Tan, Q., Chen, L., Shen, H., Yang, H., Piao, S., Wang, H., Wada, Y., 2020. Deceleration of China's human water use and its key drivers. Proc. Nat. Acad. Sci. 117 (14), 7702–7711. https://doi.org/10.1073/pnas.1909902117.

Zou, J., Zhan, C., Xie, Z., Qin, P., Jiang, S., 2016. Climatic impacts of the Middle Route of the South-to-North Water Transfer Project over the Haihe River basin in North China simulated by a regional climate model. J. Geophys. Res. 121 (15), 8983–8999. https://doi.org/10.1002/2016JD024997.